Pergamon

Acta mater. Vol. 45, No. 12, pp. 5285–5294, 1997

Printed in Great Britain
PII: S1359-6454(97)00186-9
1359-6454/97 $17.00 + 0.00

A NON-LINEAR MODEL FOR INTERNAL STRESS SUPERPLASTICITY

P. ZWIGL[1] and D. C. DUNAND[2]

[1]Department of Materials Science and Engineering, Massachusetts Institute of Technology, Cambridge, MA 02139 and [2]Department of Materials Science and Engineering, Northwestern University, Evanston, IL 60208, U.S.A.

(Received 3 April 1997)

Abstract—Most models of internal stress superplasticity predict a linear relationship between the applied stress and the plastic strain per cycle, and are only valid at low applied stresses. In the present paper, we extend the original linear theory of phase transformation superplasticity by Greenwood and Johnson [1] and derive a non-linear closed-form solution valid over the whole range of stresses, from the low-stress regime (where a linear relationship between strain and stress is predicted in agreement with the model by Greenwood and Johnson (*Proc. R. Soc. Lond.*, 1965, **283**, 403), to the high-stress regime (where the strain increases non-linearly as the applied stress approaches the yield stress of the weaker phase). The model is found to be in agreement with literature data on transformation superplasticity of iron spanning both stress regimes. Furthermore, the model is adapted to the case where internal stresses are produced by thermal expansion mismatch: it is compared to experimental literature data for metals with anisotropic thermal expansion (Zn and U) and for metal matrix composites with inhomogeneous thermal expansion (Al–SiC). © *1997 Acta Metallurgica Inc.*

1. INTRODUCTION

Internal stress superplasticity arises in polycrystalline materials upon biasing of internal mismatch stresses or strains, that are produced during a thermal excursion, by an externally applied stress. This thermal mismatch can occur (i) between grains with anisotropic coefficients of thermal expansion (CTE), e.g. in zinc [2, 3] and uranium [3, 4]; (ii) between phases with different CTE, e.g. in Al–SiC [5–7]; or (iii) between grains during a phase transformation exhibiting two allotropes with different densities, e.g. in iron [1, 8–10] and titanium [1, 11, 12]. Upon repeated thermal cycling, plastic increments can be accumulated to give large total strains (> 100%) without failure, a mechanism called CTE-mismatch superplasticity or transformation mismatch superplasticity, respectively. Depending on the homologous temperature and the nature of the material, internal stresses are relaxed either by a time-dependent mechanism at high homologous temperatures, i.e. creep, or by a time-independent mechanism at low homologous temperatures, i.e. yield.

Assuming an ideally plastic material undergoing a phase transformation, Greenwood and Johnson [1] derived an approximate analytical solution for the strain per transformation ϵ (e.g. either α-Fe to γ-Fe or γ-Fe to α-Fe) as a function of the volume mismatch $\Delta V/V$ between the two allotropic phases, the externally applied uniaxial stress σ and the yield stress σ_Y of the weaker phase:

$$\epsilon \sim \frac{5}{6}\frac{\Delta V}{V}\frac{\sigma}{\sigma_Y}. \quad (1)$$

Petsche and Stangler [13] extended the model by Greenwood and Johnson [1] qualitatively to include temperature cycle characteristics, e.g. cycle amplitude and frequency. Mitter [14] introduced a linear model incorporating the yield stress of the stronger phase. He also numerically evaluated the model of Greenwood and Johnson [1] at large values of the applied stress where he predicted a departure from the linear strain–stress relationship given in equation (1). He further formulated a micromechanical model which was used by Fischer [15] to derive a closed-form analytical solution for the strain per transformation ϵ valid at all stresses. Diani *et al.* [16] and Sato and Kuribayashi [17] developed complex theoretical models based on continuum micromechanics for transformation induced plasticity and internal stress superplasticity, respectively. Applying these models to a phase transformation with a volume mismatch under a uniaxial external stress gives linear relations between the plastic strain and the applied stress similar to equation (1). Kot and Weiss [18] developed a dislocation based model and derived an equation similar to equation (1), except that the yield stress is replaced by the internal stress owing to the transformation. Poirier [19] also derived a dislocation based model and showed that the result can be reduced to equation (1). That model was extended by Gautier *et al.* [20]

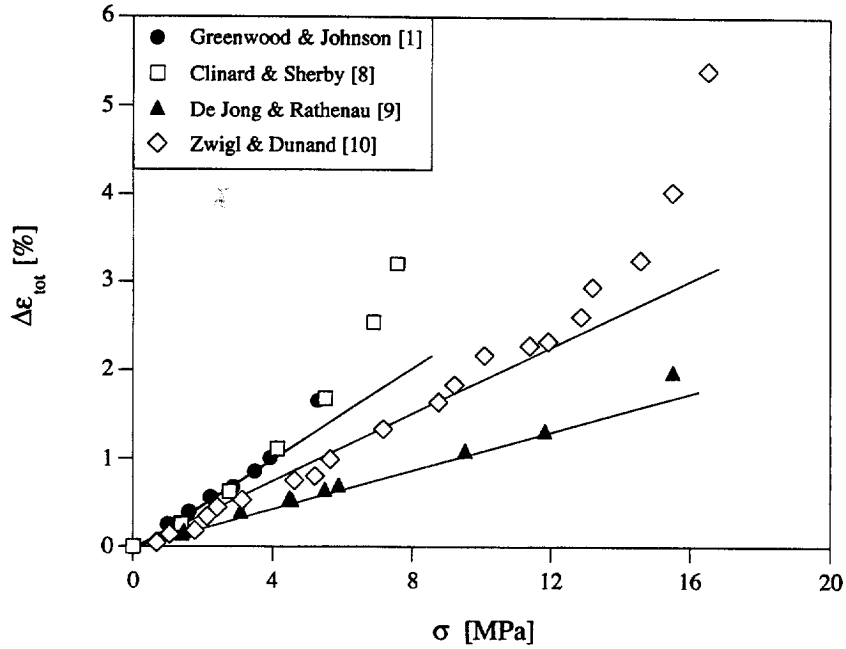

Fig. 1. Strain per cycle as a function of applied stress for iron with varying purity. Data by Clinard and Sherby [8] are creep corrected.

to include the kinetics of the phase transformation, also showing a linear relationship between plastic strain and applied stress. Other authors have treated the case of CTE-mismatch superplasticity in a similar manner, as reviewed in Ref. [7]. In summary, all existing analytical models for low-temperature phase transformation plasticity predict either a linear relationship between ϵ and σ as shown in equation (1), or a non-linear behavior using additional assumptions. The derivation by Greenwood and Johnson [1] (summarized in the Appendix) uses assumptions which limit the validity of equation (1) to small strains, i.e. $\epsilon \ll \Delta V/V$ or, equivalently, to small applied stresses, i.e. $\sigma \ll \sigma_Y$.

Greenwood and Johnson's model was tested experimentally by many investigators for allotropic metals such as iron [1, 8–10, 13], cobalt [1, 21], uranium [1], titanium [1, 11, 12], and zirconium [1]. The first three of these metals are most appropriate for comparison to equation (1), as creep is slow at their transformation temperatures and the assumption of ideal plasticity is thus accurate. Figure 1 shows literature results reported by Greenwood and Johnson [1], Clinard and Sherby [8], de Jong and Rathenau [9] and Zwigl and Dunand [10] for transformation superplasticity of iron containing little or no alloying elements. In that figure, $\Delta\epsilon_{tot}$ is defined as the strain per full thermal cycle, i.e. α–γ–α. As discussed later, the scatter between the experimental curves in Fig. 1 can be attributed to varying impurity and carbon contents in the samples investigated. In general, linear relationships are observed at small strains or stresses, in qualitative agreement with the predictions of equation (1). However, at higher strains or stresses a considerable deviation from linearity occurs. This effect could be attributed either to the transition from time-independent to time-dependent material behavior (i.e. creep) or to the breakdown of equation (1) at high stresses. Since creep is insignificant in the above experiments [1, 8–10], the non-linear behavior in Fig. 1 is an intrinsic behavior which cannot be modeled with the existing linear theories.

In the present paper, we model internal stress superplasticity of an ideal plastic material exhibiting high strains per transformation by extending Greenwood and Johnson's theory to applied stresses up to the yield stress without further assumptions. We then compare the model predictions to literature values that show non-linear transformation superplastic behavior, e.g. iron. Furthermore, we apply our model to superplasticity induced by other internal stress mechanisms, i.e. anisotropic thermal expansion mismatch and composite thermal expansion mismatch.

2. ANALYTICAL MODEL

As summarized in the Appendix, equation (1) was derived under the assumption that the plastic strain increment ϵ is much smaller than the transformation volumetric mismatch $\Delta V/V$, i.e. for small applied stresses. But if the plastic strain becomes comparable to, or even larger than the volumetric mismatch, the non-linear terms ignored by Greenwood and Johnson [1] in their derivation (see Appendix) cannot be neglected and equation (1) is invalid.

We first define dimensionless stresses and strains:

$$\alpha := \epsilon/(\Delta V/V) \tag{2}$$

$$\beta := \sigma'_{zz}/\sigma_Y \tag{3}$$

$$\gamma := (\Delta V/V)_{zz}/(\Delta V/V) \tag{4}$$

$$\delta := \sigma/\sigma_Y \tag{5}$$

where σ'_{zz} and $(\Delta V/V)_{zz}$ are defined in the Appendix. With these definitions, equation (A15) is rewritten as:

$$\beta = (\alpha - \gamma)\left(1 + \frac{9}{4}\alpha^2 - \frac{9}{2}\alpha\gamma\right)^{-1/2}. \tag{6}$$

Rather than expanding terms and linearizing the resulting expression as done by Greenwood and Johnson (see Appendix), we determine the volume average over both sides of equation (6) and use equations (3), (5) and (A17) to get:

$$\delta = \frac{(3/2)\int_\Omega (\alpha - \gamma)\left(1 + \frac{9}{4}\alpha^2 - \frac{9}{2}\alpha\gamma\right)^{-1/2} d\Omega}{\int_\Omega d\Omega} \tag{7}$$

where Ω is a spherical volume element. With $(\Delta V/V)_{zz}$ given by equations (A7)–(A10), the right hand side of equation (7) is solved analytically, giving:

$$\delta = \frac{1}{4} + \frac{1}{6\alpha} + \frac{1}{2\sqrt{2\alpha}}\left(\frac{3\alpha}{4} - \frac{1}{6} - \frac{1}{9\alpha}\right) \times \ln\left(\frac{(3\alpha + 3\sqrt{2\alpha} + 2)^2}{9\alpha^2 - 6\alpha + 4}\right). \tag{8}$$

equation (8) is obtained without the assumption of small strain ($\epsilon \ll \Delta V/V$) and is thus valid for all applied stresses below the yield stress, unlike Greenwood and Johnson's original solution [equation (1)], expressed in dimensionless form as:

$$\delta \sim \frac{6}{5}\alpha. \tag{9}$$

Figure 2 shows the solution derived by Greenwood and Johnson [equation (9)] together with the exact solution given by equation (8).

This figure shows the following characteristics:

- Despite its complexity, the exact solution [equation (8)] is almost linear for $0 < \delta < 0.5$ and follows closely the approximate linear solution by Greenwood and Johnson [equation (9)]. Surprisingly, Greenwood and Johnson's solution [equation (9)] coincides far beyond its nominal range of validity (i.e. $\alpha \ll 1$) with the exact solution [equation (8)]. This fortuitous agreement results from the quasi-linear nature of equation (8) up to $\alpha \approx 0.4$.
- The value of δ given by equation (8) and its slope at the origin are, respectively:

$$\lim_{\alpha \to 0} \delta = 0 \tag{10}$$

$$\lim_{\alpha \to 0} \frac{d\delta}{d\alpha} = \frac{6}{5} \tag{11}$$

as determined by series expansion. As expected, these values correspond to those predicted by Greenwood and Johnson [equation (9)].

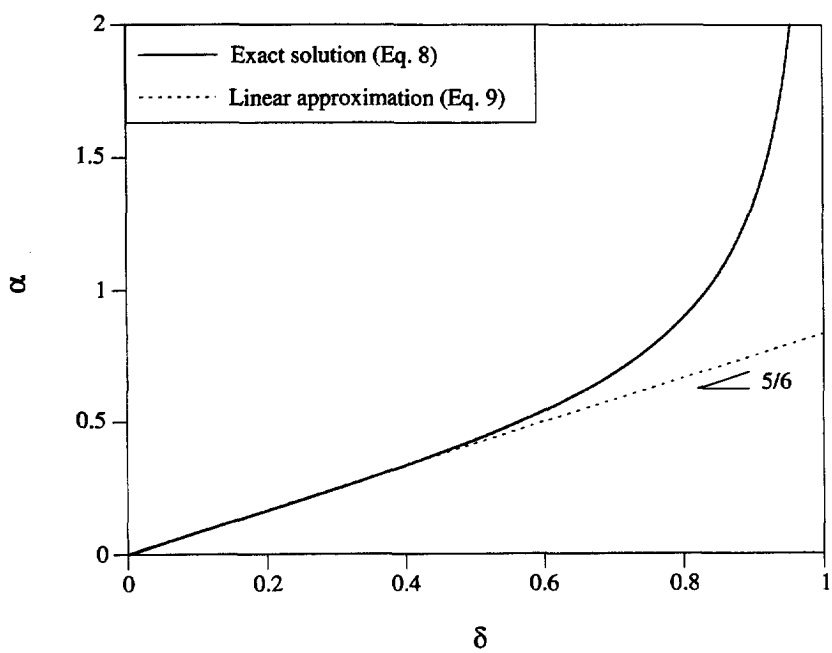

Fig. 2. Dimensionless transformation strain as a function of dimensionless applied stress as predicted by equation (8) (exact solution) and equation (9) (approximate solution by Greenwood and Johnson [1]).

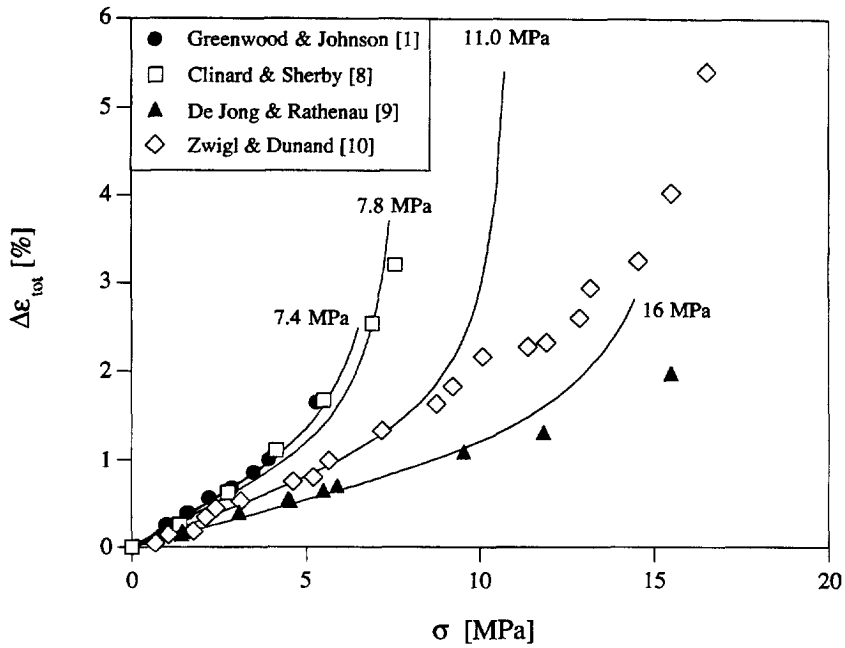

Fig. 3. Total strain per cycle as a function of applied stress. Literature values (symbols) are compared to model prediction [line, equation (8)] with σ_Y as a parameter given in the figure.

- The strains predicted by equation (8) diverge towards values larger than those extrapolated from equation (9) when the applied stress approaches the yield stress. As expected for a perfectly plastic material, the strain becomes infinite when the applied stress tends to the yield stress:

$$\lim_{\alpha\to\infty} \delta = 1. \tag{12}$$

This equation was proved by using L'Hospital rule.

3. DISCUSSION

While the above solution [equation (8)] is the same as that found by Fischer [15], equation (8) is based only on the original assumptions made by Greenwood and Johnson and does not necessitate any further hypothesis. Thus, the radial strain components introduced by Mitter [14] and Fischer [15] do not affect the final result.

3.1. Transformation superplasticity

Figure 3 shows the total strain per cycle as a function of the applied stress for experimental literature data of iron, together with predictions by equation (8). Fitting was done by keeping the volumetric mismatch constant at $\Delta V/V = 1.05\%$ [22], while changing the yield stress systematically until the sum of the squared differences between the applied and calculated stress was minimum:

$$\sum_{i=1}^{n} [\sigma_i - \sigma_Y \delta_i]^2 \stackrel{!}{=} \min \tag{13}$$

where n is the number of points measured. In Fig. 3, we assume that the strain of a full α–γ–α transformation cycle is the sum of two equal half-cycle contributions (α–γ and γ–α, respectively):

$$\Delta\epsilon_{tot} = 2\epsilon. \tag{14}$$

As shown in Fig. 3, there is good agreement between experiment and model for the data by Greenwood and Johnson [1] with a yield stress $\sigma_Y = 7.4$ MPa and the data by Clinard and Sherby [8] with $\sigma_Y = 7.8$ MPa. However, the data of de Jong and Rathenau [9] and Zwigl and Dunand [10] cannot be fitted with the single parameter σ_Y [equation (13)]. This is because in equation (8) the yield stress affects not only the non-linear behavior of the ϵ–σ curve but also the value of the slope in the linear region. Fitting only the data in the linear range gives yield stresses of 16 MPa and 11 MPa for the data by de Jong and Rathenau [9] and Zwigl and Dunand [10], respectively. In Fig. 3, the predicted curves, however, diverge at stress values that are too low; this behavior is attributed to strain hardening, as discussed in the following.

Table 1 summarizes the chemical composition of samples used by the different investigators and shows that the yield stress, σ_Y, as determined from fitting of the experimental data, tends to increase with decreasing overall purity. Furthermore, the impurity content also affects the post-yield behavior. The higher purity data by Greenwood and Johnson [1] and by Clinard and Sherby [8] can accurately be described as ideally plastic (Fig. 3), a central assumption of the models. However, samples used by de Jong and Rathenau [9] and

Table 1. Chemical composition and material parameters for the yield stress given by equation (15) for iron

Purity (wt%)	Main impurity (wt%)	σ_Y (MPa)	k	σ_t (MPa)	Reference
~100	~0	7.4	0	0	Greenwood and Johnson [1]
99.7	0.02 C	7.8	0	0	Clinard and Sherby [8]
99.7	0.3 O	11	0.51	5.5	Zwigl and Dunand [10]
~99.8	0.2 C	16	0.41	8	de Jong and Rathenau [9]

Zwigl and Dunand [10] contained 0.2% carbon and 0.3% oxygen, respectively. These impurity levels are much higher than their solubility limits, so that the resulting iron carbides and oxides, are likely to affect the plastic behavior of the matrix by increasing both the yield stress and the post-yield strain-hardening rate. Strain hardening results in yield stresses σ_Y^* after plastic deformation that are higher than the initial yield stress σ_Y. This behavior can be modeled with a simple stress criterion:

$$\sigma_Y^* = \begin{cases} \sigma_Y & \text{for } \sigma < \sigma_t \\ \sigma_Y + k(\sigma - \sigma_t) & \text{for } \sigma \geq \sigma_t \end{cases} \quad (15)$$

where σ_t is a threshold stress and k is a parameter controlling the hardening rate. Table 1 shows these optimized parameters with the threshold stress, σ_t, set as half the initial yield stress, σ_Y, determined from equation (13) and shown in Fig. 3. equation (15) thus only contains two fitting parameters, i.e. σ_Y and k. With σ_Y given by the fitting in the linear range, k is obtained by fulfilling the condition:

$$\sum_{i=1}^{n} [\sigma_i - \sigma_Y^* \delta_i]^2 \stackrel{!}{=} \min \qquad \text{for } \sigma \geq \sigma_t. \quad (16)$$

Optimal values for k are given in Table 1.

The validity of the analytical model [equation (8)] with and without strain hardening is tested by plotting the normalized stress δ [with σ_Y given by equation (15) and parameters taken from Table 1] vs the normalized strain α [with ϵ given by equation (14)]. The result is shown in Fig. 4 together with the prediction of equation (8). Given the uncertainties of the purities of the materials and differences in the cycling parameters, i.e. frequencies and temperature amplitudes, the model is in good agreement with the experimental observations.

3.2. CTE-mismatch superplasticity

equation (8) can be adapted to describe superplasticity resulting from other mismatch mechanisms, e.g. martensititic phase transformations [23, 24], irradiation swelling [25], compressibility mismatch [26] and CTE-mismatch [7]. The latter mechanism is discussed in the following, first for pure metals with anisotropic CTE, and second for metal matrix composites with inhomogeneous CTE.

The treatment developed by Greenwood and Johnson [1] can be generalized to describe mismatch superplasticity by replacing the phase transformation strain tensor ϵ_{ij}^T [equation (A6)] with a general mismatch strain tensor ϵ_{ij}^M. The internal strains [equation (A4)] then become:

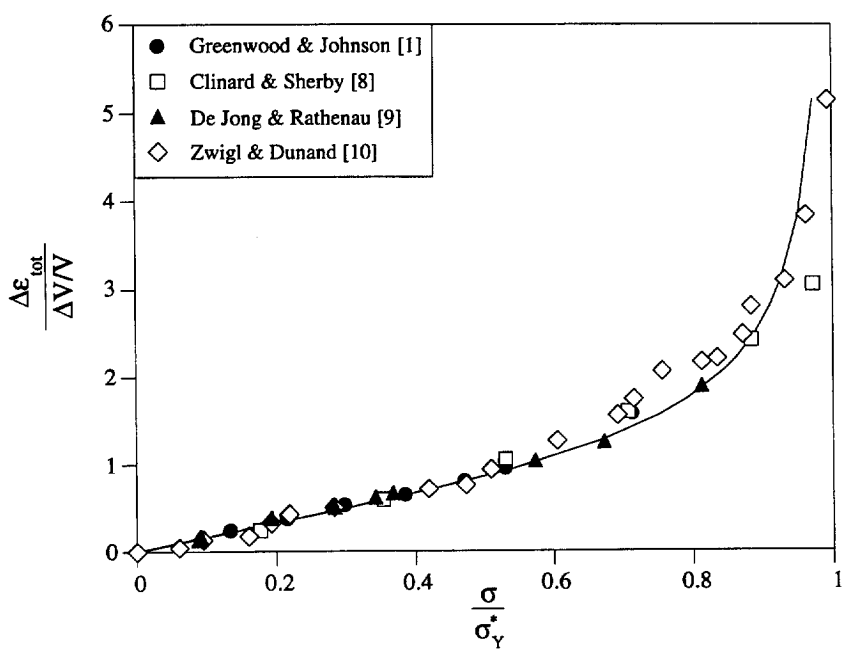

Fig. 4. Total strain per cycle normalized by the transformation mismatch strain as a function of applied stress normalized by the yield stress (symbols). Theoretical solution [equation (8)] is given by the line.

$$\epsilon_{ij} = \epsilon_{ij}^{P} + \epsilon_{ij}^{M}. \tag{17}$$

From the strain invariants, defined by the principal axes of the ϵ_{ij}^{M} tensor [27], it follows that:

$$\epsilon_{xx}^{M^2} + \epsilon_{yy}^{M^2} + \epsilon_{zz}^{M^2} + 2\left(\epsilon_{xy}^{M^2} + \epsilon_{xz}^{M^2} + \epsilon_{yz}^{M^2}\right) = \frac{2}{3}\left(\frac{\Delta V}{V}\right)_{eq}^{2} \tag{18}$$

where $(\Delta V/V)_{eq}$ is the equivalent mismatch strain producing the internal stresses. Once the equivalent mismatch strain is specified, the derivation follows that of the phase transformation plasticity presented in the Appendix, using equation (17) instead of equation (A4). The final result is again equation (8) where α is now defined as $\epsilon/(\Delta V/V)_{eq}$.

The equivalent mismatch produced by the CTE-mismatch mechanisms is of the general form:

$$\left(\frac{\Delta V}{V}\right)_{eq} = G(f)\int_{\Delta T_{pl}} \Delta\alpha \, dT \tag{19}$$

where $G(f)$ describes the dependence of the volume fraction for the case of composite CTE-mismatch ($G = 1$ for a single phase anisotropic material), $\Delta\alpha$ is the thermal expansion mismatch between the composite phases (respectively, between crystallographic directions) and ΔT_{pl} is the temperature interval which causes plasticity beyond the elastic regime. ΔT_{pl}, which is smaller than the total temperature amplitude ΔT, is a function of the CTE-difference, the elastic modulus and the yield stress of the weaker phase. Because these properties are temperature dependent, different values for ΔT_{pl} and thus $(\Delta V/V)_{eq}$ are expected for heating and cooling half-cycles, resulting in different values of half-cycle plastic strains ϵ. While it is possible to use equation (8) separately for heating and cooling half-cycles, the model can also be used with cycle-averaged values for the yield stress and ΔT_{pl}, thus assuming equal contributions for the plastic strains caused by heating and cooling. This approximate approach must be followed when analyzing strain data reported only for complete temperature cycles. In this case, equation (19) can be simplified:

$$\left(\frac{\Delta V}{V}\right)_{eq} = K\,G(f)\,\overline{\Delta\alpha}\,\overline{\Delta T_{pl}} \tag{20}$$

where K is a parameter correcting for the errors introduced by taking cycle-average values for the thermal mismatch $\overline{\Delta\alpha}\,\overline{\Delta T_{pl}}$. Thus, the closer K is to unity the better the assumptions made for $\overline{\Delta\alpha}\,\overline{\Delta T_{pl}}$ are.

3.2.1. Anisotropic CTE-mismatch superplasticity in pure metals. Internal stress superplasticity can be induced upon thermal cycling of a polycrystalline material with anisotropic CTE, as reported for α-uranium [3,4] and zinc [2,3]. Following the derivation of Young *et al.* [28], the strain deviators of an anisotropic material in a Cartesian coordinate system, $\epsilon_{x,y,z}^{M}$, are:

$$\epsilon_{x}^{M} = K_1\,\overline{\Delta T_{pl}}\,(\alpha_1 - \alpha_{av}) \tag{21}$$

$$\epsilon_{y}^{M} = K_1\,\overline{\Delta T_{pl}}\,(\alpha_2 - \alpha_{av}) \tag{22}$$

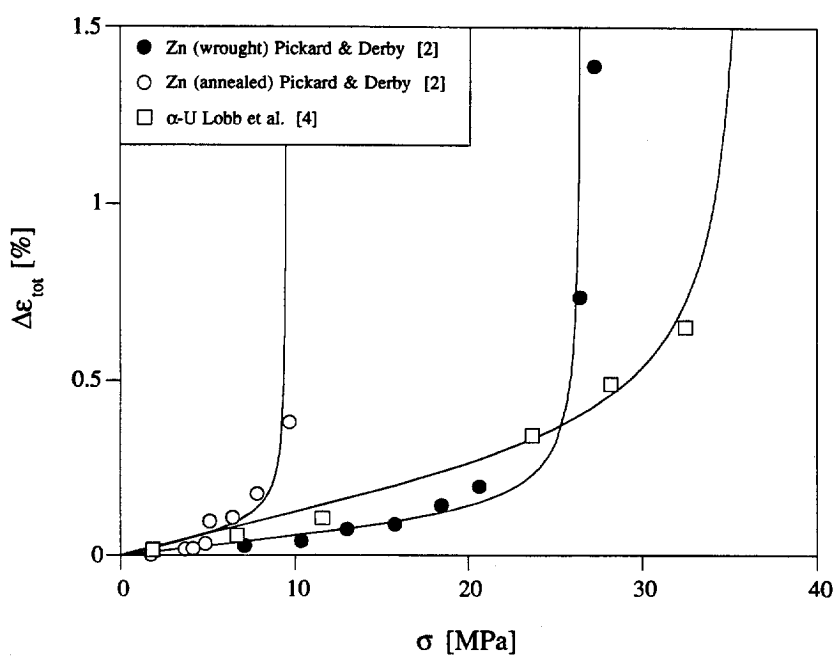

Fig. 5. Total strain per cycle as a function of applied stress for anisotropic CTE-mismatch superplasticity of α-uranium [4] and zinc [2] (symbols) compared to model predictions by equation (8) (line) using parameters given in Table 2.

Table 2. Summary of material parameters used in CTE-mismatch superplasticity models

Material	σ_Y (MPa)	$(\Delta V/V)_{eq}$ (%)	K_1 [equation (27)]	K_2 [equation (31)]	Reference
α-U	36.0	0.27	0.24	—	Lobb *et al.* [4]
Zn (wrought)	26.5	0.090	0.21	—	Pickard and Derby [2]
Zn (annealed)	9.5	0.070	0.17	—	Pickard and Derby [2]
2124 Al/20SiC$_w$	47.5	0.019	—	0.46	Chen *et al.* [6]
Pure Al/20SiC$_p$	26.0	0.082	—	2.7	Pickard and Derby [5]
Pure Al/30SiC$_p$	26.5	0.063	—	1.6	Pickard and Derby [5]

$$\epsilon_z^M = K_1 \overline{\Delta T_{pl}} (\alpha_3 - \alpha_{av}) \tag{23}$$

where α_1, α_2, α_3 are the CTEs along the crystallographic directions (which are, in general, temperature dependent), $\alpha_{av} = \frac{1}{3}(\alpha_1 + \alpha_2 + \alpha_3)$ is the average CTE of an aggregate of randomly oriented grains and K_1 is the correction parameter.

Equations (21)–(23) are equivalent to equations (A7)–(A9), given by Greenwood and Johnson [1] for transformation superplasticity. For the special cases of α-uranium and zinc, $\alpha_1 \approx \alpha_2 \neq \alpha_3$ [29], so that equations (21)–(23) become:

$$\epsilon_x^M = (1/3) K_1 \overline{\Delta\alpha_m}\, \overline{\Delta T_{pl}} \tag{24}$$

$$\epsilon_y^M = (1/3) K_1 \, overline\Delta\alpha_m \, \overline{\Delta T_{pl}} \tag{25}$$

$$\epsilon_z^M = (-2/3) K_1 \overline{\Delta\alpha_m}\, \overline{\Delta T_{pl}} \tag{26}$$

where $\overline{\Delta\alpha_m}$ is the temperature-averaged difference between α_1 and α_3. When comparing equations (24)–(26) to equations (A7)–(A9), the equivalent mismatch for the case of anisotropic CTE-mismatch plasticity is:

$$\left(\frac{\Delta V}{V}\right)_{eq} = K_1 \overline{\Delta\alpha_m}\, \overline{\Delta T_{pl}}. \tag{27}$$

The parameter K_1 can be found with equation (27) from the experimental values for $\overline{\Delta T_{pl}}$, the average CTE, $\overline{\Delta\alpha_m}$, and the equivalent mismatch $(\Delta V/V)_{eq}$ determined by fitting equation (8) to the data with the algorithm given in equation (13). The squared residuals are minimized iteratively by keeping σ_Y constant while locating the minimum for α, through changes in $(\Delta V/V)_{eq}$ and vice versa until convergence. If $\overline{\Delta T_{pl}}$ is unknown, the total cycle amplitude ΔT can be used as an upper bound for $\overline{\Delta T_{pl}}$, thereby neglecting elastic strains. Figure 5 shows literature data for α-uranium [4] and zinc [2] together with model predictions by equation (8) fitted with the parameters given in Table 2. Our model [equation (8)] successfully describes both the linear and the non-linear region of experimental data and gives two fitted parameters, σ_Y and $(\Delta V/V)_{eq}$, that are discussed in the following.

Lobb *et al.* [4] showed that the strain rates of α-uranium cycled between 400°C and 600°C (T/

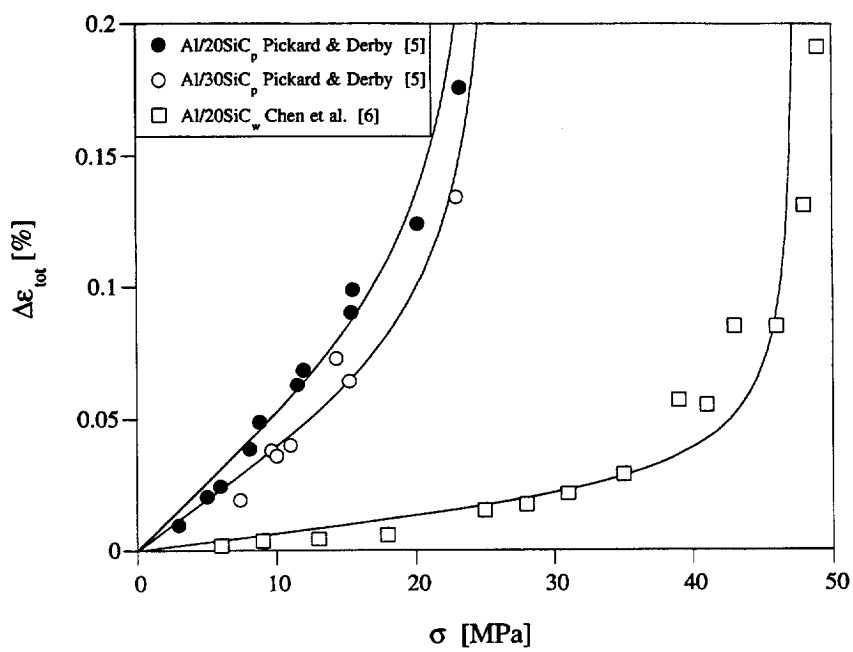

Fig. 6. Total strain per cycle as a function of applied stress for composite CTE-mismatch superplasticity of Al/SiC composites [5, 6] (symbols) compared to model predictions by equation (8) (line) using parameters given in Table 2.

$T_m = 0.48$–0.62) are significantly higher compared to the rates of isothermal creep at 600°C. Thus, plastic accommodation is by time-independent yield rather than by creep and the present model is applicable. With an average CTE-mismatch of $\overline{\Delta\alpha_m} = 55.2 \times 10^{-6}$ K^{-1} between 400°C and 600°C [29] and a temperature amplitude $\Delta T = 200K$ (an upper bound for $\overline{\Delta T_{pl}}$), a maximum mismatch of $\overline{\Delta\alpha_m}\ \Delta T = 1.1\%$ is calculated, giving a reasonable value of 0.24 for the parameter K_1. The value obtained for the yield stress ($\sigma_Y = 36$ MPa) is also reasonable in view of the yield stresses reported at 400°C ($\sigma_Y = 120$ MPa) and at 600°C ($\sigma_Y = 20$ MPa) [30].

The zinc data shown in Fig. 5 was measured by Pickard and Derby [2] on high-purity wrought zinc and the same material after annealing at 350°C. Temperature cycles were between 60°C and 150°C ($T/T_m = 0.48$–0.61) and at all temperatures the strain rates caused by thermal cycling are significantly higher than the isothermal creep rates calculated from Ref. [31]. The fitted average yield stress of the wrought material is 26.5 MPa, below the room temperature value of 33 MPa measured by Pickard and Derby [2], as expected from the negative temperature dependence of the yield stress. The annealed zinc is best fitted with a yield stress of 9.5 MPa. This value is much lower than that for the wrought material (26.5 MPa), as expected from recovery and recrystallization after annealing at a very high homologous temperature ($T/T_m = 0.90$). With $\overline{\Delta\alpha_m} = 46.8 \times 10^{-6}$ K^{-1} [29], the maximum available mismatch is $\overline{\Delta\alpha_m}\ \Delta T = 0.42\%$, leading to values for K_1 of 0.21 and 0.17, which are similar to that of α-uranium ($K_1 = 0.24$). The similarity in the values of K_1, while possibly fortuitous, is encouraging.

3.2.2. Composite CTE-mismatch superplasticity. Composites containing phases with different CTEs also exhibit mismatch superplasticity [7]. At low homologous temperatures where yield is the controlling deformation mechanism, the present model [equation (8)] can be used by fitting the yield stress and the equivalent volumetric mismatch. For CTE-mismatch superplasticity in composites, the strain deviators are:

$$\epsilon_x^M = K_2 G(f)\,\overline{\Delta\alpha}\,\overline{\Delta T_{pl}} \tag{28}$$

$$\epsilon_y^M = K_2 G(f)\,\overline{\Delta\alpha}\,\overline{\Delta T_{pl}} \tag{29}$$

$$\epsilon_z^M = -2K_2 G(f)\,\overline{\Delta\alpha}\,\overline{\Delta T_{pl}} \tag{30}$$

where $\overline{\Delta\alpha}$ is the temperature-averaged linear mismatch between the CTEs of reinforcement and matrix, $\overline{\Delta T_{pl}}$, the temperature difference causing plastic deformation, $G(f)$ a function of the reinforcement volume fraction f and K_2 the correction parameter incorporating the non-ideality of the assumptions made above. Comparing equations (28)–(30) to equations (A7)–(A9), the equivalent mismatch for composite CTE-mismatch superplasticity becomes:

$$\left(\frac{\Delta V}{V}\right)_{eq} = 3G(f)K_2\overline{\Delta\alpha}\,\overline{\Delta T_{pl}}. \tag{31}$$

Figure 6 shows the data and fits for Al/SiC metal matrix composites from Chen *et al.* [6] and Pickard and Derby [5]. Chen *et al.* [6] cycled a 2124 Al composite containing 20 vol.% SiC whiskers between 100°C and 350°C ($T/T_m = 0.40$–0.67) and showed that the strain rates caused by thermal cycling are more than an order of magnitude higher than isothermal creep at a homologous temperature of 0.69. Pickard and Derby [5] used composites containing 20 vol.% and 30 vol.% 2.3 μm SiC particles with a matrix of commercially pure aluminum, for which plasticity by creep was also insignificant over the cycling temperature range between 130°C and 350°C ($T/T_m = 0.43$–0.67). Thus the composite behavior upon thermal cycling is controlled by time-independent yield and can be described by equation (8) with $(\Delta V/V)_{eq}$ given by equation (31). The fitted values for σ_Y and $(\Delta V/V)_{eq}$ are given in Table 2.

Table 2 shows that the yield stress is significantly higher for the composite with an alloyed 2124 matrix than for the pure aluminum composite. This effect is expected both because the alloy is stronger than the pure metal and because whiskers typically strain harden a metallic matrix more effectively than particles. Also, Pickard and Derby [5] measured the yield stress of the commercially pure aluminum matrix as a function of the temperature, giving a cycle-averaged yield stress of 20.5 MPa, in reasonable agreement with our fitted values of 26 MPa for the 20 vol.% SiC_p composite and 26.5 MPa for the 30 vol.% SiC_p.

The dependence of the volume fraction was modeled by Pickard and Derby [5] as $G(f) = (1-f)f$. Furthermore, they independently measured the temperature amplitude ΔT_{el} for the onset of plasticity. By taking $\overline{\Delta\alpha_m} = 22.7 \times 10^{-6}$ K^{-1} [29] and an average value for heating and cooling $\overline{\Delta T_{el}} = 137$ K (i.e. $\overline{\Delta T_{pl}} = \Delta T - \overline{\Delta T_{el}} = 83$ K), the mismatch strains are $3G(f)\,\overline{\Delta\alpha_m}\,\overline{\Delta T_{pl}} >= 0.030\%$ and 0.040% for the 20 vol.% and 30 vol.% SiC_p composite, respectively. Using the fitted values for $(\Delta V/V)_{eq}$ given in Table 2, K_2 values of 2.7 and 1.6, respectively, are obtained from equation (31). Assuming the same value for $\Delta T_{el} = 137$ K, the mismatch strain of the 2124 Al composite becomes 0.041% and $K_2 = 0.46$. While K_2 values are similar for the two pure aluminum composites, the value for K_2 for the alloyed composite is significantly lower, possibly because (i) the yield stress of the 2124 alloy is much higher than for pure aluminum, thus increasing ΔT_{el}, and (ii) whiskers produce a mismatch stress field different from that of equiaxed particles.

In general, the values for the correcting parameters K_1 and K_2 determined for anisotropic CTE-

mismatch and composite mismatch superplasticity are, respectively, within factors of 6 and 3 of the predicted ideal value of unity. We believe that this error can be explained by the assumptions and approximations made for the equivalent mismatch [equation (20)].

4. CONCLUSIONS

Allotropic materials deforming by transformation superplasticity exhibit at low applied stresses a linear relationship between plastic strain per transformation and the applied stress, as predicted by the linear relationship of Greenwood and Johnson [1]. However, at intermediate and high applied stresses, where their theory becomes invalid, experimental data show that the strain increases non-linearly with the applied stress. We generalize the original theory of Greenwood and Johnson [1] to include these stress regimes and derive a closed-form solution valid for all applied stresses (from zero up to the yield stress of the weaker phase) for an ideally plastic material. As expected, the strains predicted by the complete solution converge to the linear expression by Greenwood and Johnson [1] at low stresses and diverge to infinity for stresses tending towards the yield stress. The complete solution accurately describes data for high-purity iron in both these linear and non-linear regions. The model is then extended to the case of a strain-hardening material and applied successfully to literature data for iron with high impurity content. Finally, the model is adapted to the more complex case of CTE-mismatch superplasticity exhibited by metals with anisotropic CTE and by composites with inhomogeneous CTE. Experimental literature data on α-uranium, zinc and Al–SiC composites are successfully described with two fitting parameters (yield stress and thermal mismatch) which take values that are physically reasonable.

Acknowledgements—This study was supported by the US Army Research Office under grant DAAH004-95-1-0629 monitored by Dr W.C. Simmons.

REFERENCES

1. Greenwood, G. W. and Johnson R. H., *Proc. R. Soc. Lond.*, 1965, **283**, 403.
2. Pickard, S. M. and Derby, B., *Scripta metall.*, 1991, **25**, 467.
3. Wu, M. Y., Wadsworth, J. and Sherby, O. D., *Metall. Trans. A*, 1987, **18A**, 451.
4. Lobb, R. C., Sykes, E. C. and Johnson, R. H., *Metal Sci. J.*, 1972, **6**, 33.
5. Pickard, S. M. and Derby, B., *Acta metall.*, 1990, **38**, 2537.
6. Chen, Y-C., Daehn, G. S. and Wagoner, R. H., *Scripta metall.*, 1990, **24**, 2157.
7. Dunand, D. C. and Derby, B., *Fundamentals of Metal-Matrix Composites*, ed. S. Suresh, A. Mortensen and A. Needleman. Butterworth–Heineman, Boston, 1993, p. 191.
8. Clinard, F. W. and Sherby, O. D., *Acta metall.*, 1964, **12**, 911.
9. de Jong, M. and Rathenau, G. W., *Acta metall.*, 1959, **7**, 246.
10. Zwigl, P. and Dunand, D. C., submitted to *Metall. Trans.*
11. Chaix, C. and Lasalmonie, A., *Res Mech.*, 1981, **2**, 241.
12. Dunand, D. C. and Bedell, C. M., *Acta metall.*, 1996, **44**, 1063.
13. Petsche, S. and Stangler, F., *Z. Metallk.*, 1971, **62**, 601.
14. Mitter, W., *Umwandlungsplastizität und ihre Berücksichtigung bei der Berechnung von Eigenspannungen*. Gebr. Bornträger, Berlin, 1987, p. 40.
15. Fischer, F. D., *Acta metall.*, 1990, **8**, 1535.
16. Diani, J. M., Sabar, H. and Berveiller, M., *Int. J. Engng Sci.*, 1995, **33**, 1921.
17. Sato, E. and Kuribayashi, K., *Acta metall.*, 1993, **41**, 1759.
18. Kot, R. A. and Weiss, V., *Metall. Trans.*, 1970, **1**, 2685.
19. Poirier, J. P., *J. Geophys. Res.*, 1982, **87**, 6791.
20. Gautier, E., Simon, A. and Beck, B., *Acta metall.*, 1987, **35**, 1367.
21. Zamora, M. and Poirier, J. P., *Mech. Mater.*, 1983, **2**, 193.
22. Basinski, Z. S., Hume-Rothery, W. and Sutton, A. L., *Proc. R. Soc. Lond.*, 1955, **229**, 459.
23. Gautier, E. and Simon, A., *Phase Transformations '87*, Institute of Metals, Cambridge, 1987, p. 285.
24. Porter, L. F. and Rosenthal, P. C., *Acta. metall.*, 1959, **7**, 504.
25. Roberts, A. C. and Cottrell, A. H., *Phil. Mag.*, 1956, **1**, 711.
26. Huang, C. Y. and Daehn, G. S., *Superplasticity and Superplastic Forming 1995*. TMS, Warrendale PA, 1996, p. 135.
27. Dieter, G. E., *Mechanical Metallurgy*. McGraw-Hill Book Company, New York, 1976, p. 35.
28. Young, A. G., Gardiner, K. M. and Rotsey, W. B., *J. Nucl. Mater.*, 1960, **2**, 234.
29. Touloukian, Y. S., Kirby, R. K., Taylor, R. E. and Desai P. D. (eds), *Thermal Expansion*, Vol. 2, IFI/Plenum, New York, 1975.
30. Sherby, O. D., Bly, D. L. and Wood, D. H., *Physical Metallurgy of Uranium Alloys*. ed. J. J. Burke. Columbus, 1976, p. 311.
31. Frost, H. J. and Ashby, M. F., *Deformation-Mechanism Maps*. Pergamon Press, New York, 1982.
32. Anderson, R. G. and Bishop, J. F. W., in *Symp. Uranium and Graphite*, Institute of Metals, London, 1962, p. 17.

APPENDIX A: SUMMARY OF THE DERIVATION BY GREENWOOD AND JOHNSON [1]

Phase transformation superplasticity is attributed to the presence of deviatoric stresses $\sigma_{ij}=\sigma_{ij}-(1/3)\delta_{ij}\sigma_{kk}$ where σ_{ij} are the stress tensor components, σ_{kk} its hydrostatic components and δ_{ij} the Kronecker symbol. The kinetics of strain production is modeled as

$$\dot{\epsilon}_{ij} = \sigma'_{ij}\lambda \tag{A1}$$

where $\dot{\epsilon}_{ij}$ are the internal strain rate components and $1/\lambda$ is the viscosity of the weaker phase once the yield stress is reached. Assuming that the rate of production of the internal stress is fast compared to any possible relaxation mechanism, equation (A1) can be integrated over the time

of transformation Δt to give:

$$\epsilon_{ij} = \sigma'_{ij}\lambda_1 \tag{A2}$$

where $\lambda_1 = \lambda\Delta t$ is a constant. The internal strain components ϵ_{ij} are only a function of the deviatoric stress components. Substituting equation (A2) into the Lévy–von Mises yield criterion (which relates the deviatoric stress components to the yield stress, σ_Y, as measured in uniaxial tension) gives:

$$\epsilon_{xx}^2 + \epsilon_{yy}^2 + \epsilon_{zz}^2 + 2\epsilon_{xy}^2 + 2\epsilon_{yz}^2 + 2\epsilon_{xz}^2 = (2/3)\lambda_1^2\sigma_Y^2. \tag{A3}$$

The internal strains are obtained by superimposing the strains owing to plastic deformation of the weaker phase, ϵ_{ij}^P, and the strains associated with the phase transformation, ϵ_{ij}^T:

$$\epsilon_{ij} = \epsilon_{ij}^P + \epsilon_{ij}^T \tag{A4}$$

with

$$\epsilon_{ij}^P = \begin{bmatrix} -\frac{1}{2}\epsilon & 0 & 0 \\ 0 & -\frac{1}{2}\epsilon & 0 \\ 0 & 0 & \epsilon \end{bmatrix} \tag{A5}$$

$$\epsilon_{ij}^T = -\begin{bmatrix} (\Delta V/V)_{xx} & (\Delta V/V)_{xy} & (\Delta V/V)_{xz} \\ (\Delta V/V)_{xy} & (\Delta V/V)_{yy} & (\Delta V/V)_{zy} \\ (\Delta V/V)_{xz} & (\Delta V/V)_{zy} & (\Delta V/V)_{zz} \end{bmatrix} \tag{A6}$$

where ϵ is the plastic strain increment in the direction of the uniaxial applied stress and $(\Delta V/V)_{ij}$ the components of the phase transformation strain tensor. The negative sign in equation (A6) indicates that a volume reduction occurs during the phase transformation. Greenwood and Johnson [1] followed Anderson and Bishop [32] by assuming that the strain deviators $(\Delta V/V)_{x,y,z}$ in principal coordinates are:

$$(\Delta V/V)_x = (1/3)(\Delta V/V) \tag{A7}$$

$$(\Delta V/V)_y = (1/3)(\Delta V/V) \tag{A8}$$

$$(\Delta V/V)_z = (-2/3)(\Delta V/V). \tag{A9}$$

The components of the transformation strain tensor [equation (A6)] are related to the principal strain deviators [equations (A7)–(A9)] by a coordinate transformation, e.g.

$$(\Delta V/V)_{zz} = (\Delta V/V)_x \cos(\varphi)^2 \sin(\vartheta)^2 + (\Delta V/V)_y \sin(\varphi)^2 \sin(\vartheta)^2 + (\Delta V/V)_z \cos(\vartheta)^2. \tag{A10}$$

Using equations (A7)–(A9) and equation (A10), the second invariant of the transformation tensor [equation (A6)] is

$$(\Delta V/V)_{xx}^2 + (\Delta V/V)_{yy}^2 + (\Delta V/V)_{zz}^2 + 2[(\Delta V/V)_{xy}^2 + (\Delta V/V)_{xz}^2 + (\Delta V/V)_{yz}^2] = \frac{2}{3}\left(\frac{\Delta V}{V}\right)^2. \tag{A11}$$

Further, the first invariant of the phase transformation strain tensor requires that:

$$(\Delta V/V)_{xx} + (\Delta V/V)_{yy} + (\Delta V/V)_{zz} = 0. \tag{A12}$$

Introducing equation (A4) into equation (A3) and using equations (A11) and (A12) gives:

$$(3/2)\epsilon^2 - 3\epsilon(\Delta V/V)_{zz} + (2/3)(\Delta V/V)^2 = (2/3)\lambda_1^2\sigma_Y^2. \tag{A13}$$

Compatibility of strains in the z-direction (i.e. the direction of the uniaxial applied stress) requires that

$$\epsilon_{zz} \stackrel{!}{=} \epsilon - (\Delta V/V)_{zz}. \tag{A14}$$

After introducing equations (A2) and (A14) into equation (A13), eliminating λ_1 and rearranging terms, the deviatoric stress component in the z-direction is given by

$$\sigma'_{zz} = \frac{\sigma_Y[\epsilon - (\Delta V/V)_{zz}]}{(\Delta V/V)\left[1 + \frac{9\epsilon^2}{4(\Delta V/V)^2} - \frac{9\epsilon(\Delta V/V)_{zz}}{2(\Delta V/V)^2}\right]^{1/2}}. \tag{A15}$$

This is equation (7) of Greenwood and Johnson's article [1]. Under the assumption that $\epsilon \ll \Delta V/V$, these authors make three approximations by:

- neglecting the ϵ^2 term in the denominator of equation (A15),
- expanding $(1-x)^{-1/2} \approx 1 + x/2$ where

$$x = \frac{9\epsilon(\Delta V/V)_{zz}}{2(\Delta V/V)^2}$$

- neglecting again the ϵ^2 term

to obtain

$$\sigma'_{zz} \sim \frac{\sigma_Y\left[\epsilon\left(1 - \frac{9(\Delta V/V)_{zz}^2}{4(\Delta V/V)^2}\right) - (\Delta V/V)_{zz}\right]}{(\Delta V/V)}. \tag{A16}$$

To get macroscopic values for stress and strain, an average over a spherical volume element Ω, integrated over ϑ, $\varphi \epsilon [0;\pi/2]$, is now applied to equation (A16). Individual integrals give:

$$\frac{\int \sigma'_{zz}\,d\Omega}{\int d\Omega} = \frac{2}{3}\sigma \tag{A17}$$

$$\frac{\int \left(\frac{\Delta V}{V}\right)_{zz}^2 d\Omega}{\int d\Omega} = \frac{4}{45}\left(\frac{\Delta V}{V}\right)^2 \tag{A18}$$

$$\frac{\int \left(\frac{\Delta V}{V}\right)_{zz} d\Omega}{\int d\Omega} = 0 \tag{A19}$$

where σ is the applied stress in the z-direction. Introducing equations (A17)–(A19) into equation (A16) leads to the concise result found by Greenwood and Johnson [1]:

$$\epsilon \sim \frac{5}{6}\frac{\Delta V}{V}\frac{\sigma}{\sigma_Y}. \tag{A20}$$